

Light mediators in dark matter direct detections

Tai Li^{*}, Sen Miao[†] and Yu-Feng Zhou[‡]

*State Key Laboratory of Theoretical Physics,
Kavli Institute for Theoretical Physics China,
Institute of Theoretical Physics, Chinese Academy of Sciences
Beijing, 100190, P.R. China*

Abstract

In an extended effective operator framework, we investigate in detail the effects of light mediators on the event spectra of dark matter (DM)-nucleus scatterings. The presence of light mediators changes the interpretation of the current experimental data, especially the determination of DM particle mass. We show by analytic and numerical illustrations that in general for all the operators relevant to spin-independent scatterings, the DM particle mass allowed by a given set of experimental data increases significantly when the mediator particle becomes lighter. For instance, in the case of CDMS-II-Si experiment, the allowed DM particle mass can reach ~ 50 (100) GeV at 68% (90%) confidence level, which is much larger than ~ 10 GeV in the case with contact interactions. The increase of DM particle mass saturates when the mediator mass is below $\mathcal{O}(10)$ MeV. The upper limits from other experiments such as SuperCDMS, CDMSlite, CDEX, XENON10/100, LUX, PandaX etc. all tend to be weaker toward high DM mass regions. In a combined analysis, we show that the presence of light mediators can partially relax the tension in the current results of CDMS-II-Si, SuperCDMS and LUX.

^{*}Email: litai@itp.ac.cn

[†]Email: miaosen@itp.ac.cn

[‡]Email: yfzhou@itp.ac.cn

1 Introduction

Weakly interacting massive particles (WIMPs) are popular candidates for dark matter (DM) which contributes to 26.8% of the energy budget of the Universe [1]. At present numerous underground DM direct detection experiments are searching for possible signals arising from the interactions between WIMPs and the Standard Model (SM) particles.

In the recent years, a number of experiments such as DAMA [2, 3], CoGeNT [4–6], and CDMS-II-Si [7] have reported possible signals in excess of known backgrounds. Other experiments, such as CDMS-II-Ge [8, 9], CDMSlite [10], SuperCDMS [11], XENON10 [12], XENON100 [13], LUX [14], PandaX [15], SIMPLE [16], and CDEX [17], etc. only reported upper limits on the scattering cross section. The recent results of CDMS-II-Si, if interpreted in terms of DM-nucleus elastic scattering in simple benchmark DM models, favor a DM particle mass ~ 8.5 GeV and a spin-independent DM-nucleon scattering cross section $\sim 2 \times 10^{-41}$ cm², which is in tension with the limits of other experiment such as SuperCDMS and LUX. Note that in the interpretation of the experimental data, the interactions between DM particles and target nuclei are often assumed to be contact, elastic, isospin conserving, momentum and velocity independent, etc.. Simplified assumptions are also adopted on the DM velocity distribution, DM local energy density, nuclear form factors, detector responses, etc.. The interpretation of the experimental data can be changed dramatically if any of the assumptions is modified.

In some DM models the interaction between DM particle and target nuclei is of long-range type through the exchange of light mediator particles. The mediator can be the SM photon if the DM particle carries tiny effective electric charge [18–20], or electric/magnetic dipole moments [21–34], or anapole moment [35–38]. Another example of the mediator particle is a massive dark photon, a hidden sector $U(1)$ gauge boson interacting with the SM particles through kinetically mixing with the SM photon (for reviews, see e.g. Refs. [39–41]). The mediator can also be a scalar particle interacting with SM fermions [42–46]. The recently observed excess in cosmic-ray positron fraction by PAMELA [47, 48], Fermi-LAT [49] and AMS-02 [50], if interpreted in terms of halo DM annihilation, requires a DM annihilation cross section significantly larger than the typical thermal DM annihilation cross section (see e.g. [51, 52]). The presence of light mediators can lead to long-range attractive forces between DM particles, which enhance the DM annihilation cross sections at low temperatures through the mechanism of Sommerfeld enhancement [53–63]. Furthermore, the DM self-interactions with light mediator mass around $\mathcal{O}(1 - 100)$ MeV can help in understanding the problems in small-scale structure (core vs. cusp) of the DM profile of dwarf galaxies [64–66].

In the light mediator scenario, the spectra of the recoil event rate are expected to be enhanced at low momentum transfer, which depends on both the type of the interaction

and the mass of the mediator. The DM interpretation of the experimental data can be significantly different from the case of contact interactions. In this work, we investigate the effects of light mediator on the interpretation of the current experimental data, especially on the determination of DM particle mass in an extended effective operator framework [67–70]. According to the momentum and velocity dependencies, the effective operators are catalogued into six types. Using analytical and numerical illustrations, we show that in general the allowed DM particle mass from the experimental data increases significantly when the mediator particle becomes lighter. For the data of CDMS-II-Si, the allowed DM particle mass can reach ~ 50 (100) GeV at 68% (90%) confidence level (CL), depending on the type of operators, and the increase saturates when the mediator mass is below $\mathcal{O}(10)$ MeV. The upper limits from other experiments such as SuperCDMS, CDMSlite, CDEX, XENON10/100, LUX, PandaX etc. all become weaker toward high DM mass region. At present, the most stringent limits are from the results of SuperCDMS and LUX, which can be marginally consistent with that of CDMS-II-Si in DM models with xenophobic interactions. We perform a combined analysis on the data of CDMS-II-Si, SuperCDMS and LUX and show that the presence of a light mediator can partially relax the tension in the current results of CDMS-II-Si, SuperCDMS and LUX.

This paper is organized as follows. In Section 2, we overview the extended effective operator approach in the presence of light mediators, and discuss the momentum and velocity dependences of the differential cross sections for all the operators. In Section 3, we discuss the effect of light mediator on the determination of DM properties, especially the mass of DM particles. In Section 4, we discuss the interpretation of the current experimental data of CDMS-II-Si, SuperCDMS, LUX and other experiments. The conclusions are given in Section 5.

2 Effective operators with a light mediator particle

In many DM models, the DM particle χ can scatter off a target nucleon $N = (p, n)$ in an elastic process $\chi(\mathbf{p}_1) + N(\mathbf{p}_2) \rightarrow \chi(\mathbf{p}_3) + N(\mathbf{p}_4)$ via exchanging a mediator particle ϕ in t -channel. For fermionic DM particles, if the mass of the mediator m_ϕ is much larger than the 3-momentum transfer $q = |\mathbf{q}| = |\mathbf{p}_3 - \mathbf{p}_1|$ of the scattering process, i.e., $m_\phi^2 \gg q^2$, the interactions responsible for the scattering can be effectively described by a set of local Lorentz-invariant operators

$$\mathcal{O}_i = \frac{c_i}{\Lambda^2} (\bar{\chi} \Gamma_i \chi) (\bar{N} \Gamma'_i N), \quad (1)$$

where Λ is the mass scale of the mediator particle, and c_i are the coefficients. The matrices Γ_i, Γ'_i are Lorentz-invariant combinations of the Dirac matrices

$$\Gamma_i, \Gamma'_i = \{1, \gamma^5, \gamma^\mu, \gamma^\mu \gamma^5, \sigma^{\mu\nu}, \sigma^{\mu\nu} \gamma^5\}.$$

When the mediator is relatively light, the correction to the effective operator approach can be made by a replacement $\Lambda^2 \rightarrow (q^2 + m_\phi^2)$, arising from the t -channel ϕ -exchange. For fermionic DM particles, up to dimension six, the operators with scalar and pseudo-scalar interactions are

$$\begin{aligned} \mathcal{O}_1 &= \frac{1}{q^2 + m_\phi^2} \bar{\chi} \chi \bar{N} N, & \mathcal{O}_2 &= \frac{1}{q^2 + m_\phi^2} \bar{\chi} \gamma^5 \chi \bar{N} N, \\ \mathcal{O}_3 &= \frac{1}{q^2 + m_\phi^2} \chi \chi \bar{N} \gamma^5 N, & \mathcal{O}_4 &= \frac{1}{q^2 + m_\phi^2} \bar{\chi} \gamma^5 \chi \bar{N} \gamma^5 N. \end{aligned} \quad (2)$$

The operators with vector or axial-vector interactions are

$$\begin{aligned} \mathcal{O}_5 &= \frac{1}{q^2 + m_\phi^2} \bar{\chi} \gamma^\mu \chi \bar{N} \gamma_\mu N, & \mathcal{O}_6 &= \frac{1}{q^2 + m_\phi^2} \bar{\chi} \gamma^\mu \gamma^5 \chi \bar{N} \gamma_\mu N, \\ \mathcal{O}_7 &= \frac{1}{q^2 + m_\phi^2} \bar{\chi} \gamma^\mu \chi \bar{N} \gamma_\mu \gamma^5 N, & \mathcal{O}_8 &= \frac{1}{q^2 + m_\phi^2} \bar{\chi} \gamma^\mu \gamma^5 \chi \bar{N} \gamma_\mu \gamma^5 N, \end{aligned} \quad (3)$$

and that with tensor interactions are

$$\mathcal{O}_9 = \frac{1}{q^2 + m_\phi^2} \bar{\chi} \sigma^{\mu\nu} \chi \bar{N} \sigma_{\mu\nu} N, \quad \mathcal{O}_{10} = \frac{1}{q^2 + m_\phi^2} \bar{\chi} \sigma^{\mu\nu} \gamma^5 \chi \bar{N} \sigma_{\mu\nu} N. \quad (4)$$

Note that other combinations of the tensor operators are not independent due to the identity $\sigma^{\mu\nu} \gamma^5 = (i/2) \epsilon^{\mu\nu\alpha\beta} \sigma_{\alpha\beta}$. If the DM particles are Majorana, the vector and tensor operators are vanishing identically. Similarly, if the DM particles are complex scalars, possible operators up to dimension six are

$$\begin{aligned} \mathcal{O}_{11} &= \frac{2m_\chi}{q^2 + m_\phi^2} \chi^* \chi \bar{N} N, & \mathcal{O}_{12} &= \frac{2m_\chi}{q^2 + m_\phi^2} \chi^* \chi \bar{N} \gamma^5 N, \\ \mathcal{O}_{13} &= \frac{1}{q^2 + m_\phi^2} (\chi^* \overleftrightarrow{\partial}_\mu \chi) \bar{N} \gamma^\mu N, & \mathcal{O}_{14} &= \frac{1}{q^2 + m_\phi^2} (\chi^* \overleftrightarrow{\partial}_\mu \chi) \bar{N} \gamma^\mu \gamma^5 N. \end{aligned} \quad (5)$$

For real scalar DM particle, the vector operators $\mathcal{O}_{13,14}$ vanish identically. Throughout this work, for simplicity, we assume that one of the operators dominates the scattering processes at a time. It is straight forward to extend the analysis to the processes involving multiple operators simultaneously.

The differential cross section for χN scattering can be written as

$$\frac{d\sigma_N}{dq^2}(q^2, v) = \frac{|\overline{\mathcal{M}_{\chi N}}|^2}{64\pi m_N^2 m_\chi^2 v^2}, \quad (6)$$

where $|\overline{\mathcal{M}_{\chi N}}|^2$ is the squared matrix element averaged over the spins of initial states, and $v = |\mathbf{v}| = |\mathbf{p}_1/m_\chi - \mathbf{p}_2/m_N|$ is the velocity of the DM particle in the nucleon rest frame. In general, the differential cross section $d\sigma_N/dq^2$ depends on both q^2 and v , and can be divergent in the limit of $q^2 \rightarrow 0$, when the mass of the mediator is vanishing. The total DM-nucleon scattering cross section σ_N are defined as the integration of $d\sigma_N/dq^2$ over q^2 in the interval from an infrared cutoff q_{\min}^2 to the maximal value allowed by kinematics $q_{\max}^2 = 4\mu_{\chi N}^2 v^2$

$$\sigma_N(v) = \int_{q_{\min}^2}^{4\mu_{\chi N}^2 v^2} dq^2 \frac{d\sigma_N}{dq^2}(q^2, v), \quad (7)$$

where $\mu_{\chi N} = m_\chi m_N / (m_\chi + m_N)$ is the DM-nucleon reduced mass. The value of q_{\min}^2 can be related to the energy threshold of DM detection experiment which is typically at keV scale.

Since $\sigma_N(v)$ is in general a function of v , it is useful to define a velocity-independent cross section $\bar{\sigma}_N$ which is the total cross section at a reference velocity v_{ref} , i.e., $\bar{\sigma}_N \equiv \sigma_N(v_{\text{ref}})$. The value of v_{ref} can be chosen to be the typical velocity of halo DM particles $\sim 200 \text{ km} \cdot \text{s}^{-1}$. Thus the differential cross section can be rewritten in the conventional form

$$\frac{d\sigma_N}{dq^2}(q^2, v) \equiv \frac{\bar{\sigma}_N}{4\mu_{\chi N}^2 v^2} G(q^2, v), \quad (8)$$

where

$$G(q^2, v) = \frac{(q_{\text{ref}}^2 - q_{\min}^2) |\overline{\mathcal{M}_{\chi N}(q^2, v)}|^2}{\int_{q_{\min}^2}^{q_{\text{ref}}^2} dq^2 |\overline{\mathcal{M}_{\chi N}(q^2, v_{\text{ref}})}|^2}, \quad (9)$$

is a factor containing the q^2 -dependence and the rest of v -dependence, and $q_{\text{ref}}^2 \equiv 4\mu_{\chi N}^2 v_{\text{ref}}^2$. It is clear that $G(q^2, v) = 1$, when the matrix element $\mathcal{M}_{\chi N}$ is a constant.

The DM models often contribute directly to one of a combination of the above mentioned Lorentz-invariant relativistic operators. In the nonrelativistic limit, the matrix element $\mathcal{M}_{\chi N}(q^2, v)$ can be expressed in terms of the products of independent Galilean invariant vectors such as the 3-momentum transfer \mathbf{q} , the transverse velocity of the DM particle $\mathbf{v}_\perp \equiv \mathbf{v} + \mathbf{q}/(2\mu_{\chi N})$, and the spin of DM particle (nucleon) \mathbf{S}_χ (\mathbf{S}_N). An important property of the transverse velocity is that it is perpendicular to \mathbf{q} in elastic χN scatterings, $\mathbf{v}_\perp \cdot \mathbf{q} = 0$ and in this case the value of v_\perp is given by

$$v_\perp^2 = v^2 - \frac{q^2}{4\mu_{\chi N}^2}. \quad (10)$$

Detailed discussions related to the properties of \mathbf{v}_\perp and nonrelativistic operators can be found in Refs. [69, 70]. In this work, we focus on the spin-independent cross sections which involve q^2 and v_\perp^2 only. According to the v_\perp^2 and q^2 dependences, the operators in Eqs. (2)–(5) can be catalogued into the following six types:

Type-I operators \mathcal{O}_1 , \mathcal{O}_5 , \mathcal{O}_{11} and \mathcal{O}_{13} correspond to scalar or vector type interactions. These operators contribution to the matrix elements with the form

$$|M_{\chi N}(q^2, v)|^2 \propto \frac{1}{(q^2 + m_\phi^2)^2}. \quad (11)$$

For type-I operators, the factor $G(q^2, v)$ is

$$G_1(q^2) = \frac{1}{I_1(q_{\min}^2/m_\phi^2, q_{\text{ref}}^2/m_\phi^2) (1 + q^2/m_\phi^2)^2}, \quad (12)$$

where the function $I_1(a, b)$ is defined as

$$I_1(a, b) \equiv \frac{1}{b-a} \int_a^b dt \frac{1}{(1+t)^2} = \frac{1}{(1+a)(1+b)}. \quad (13)$$

In the limit

$$q_{\min}^2 \ll q_{\text{ref}}^2 \ll m_\phi^2, \quad (14)$$

the function I_1 can be approximated by $I_1 \approx 1 - q_{\text{ref}}^2/m_\phi^2$. It is evident that for a heavy mediator, $q_{\text{ref}}^2, q^2 \ll m_\phi^2$, $G_1(q^2) \approx 1$, as expected.

Type-II operators \mathcal{O}_2 and \mathcal{O}_{10} contribute to the matrix elements of the form

$$|M_{\chi N}(q^2, v)|^2 \propto \frac{q^2}{(q^2 + m_\phi^2)^2}. \quad (15)$$

For type-II operators, the corresponding factor is

$$G_2(q^2) = \frac{q^2/m_\phi^2}{I_2(q_{\min}^2/m_\phi^2, q_{\text{ref}}^2/m_\phi^2) (1 + q^2/m_\phi^2)^2}, \quad (16)$$

where

$$I_2(a, b) \equiv \frac{1}{b-a} \int_a^b dt \frac{t}{(1+t)^2} = \frac{1}{b-a} \ln \left(\frac{1+b}{1+a} \right) - I_1(a, b). \quad (17)$$

In the limit of Eq. (14), the function I_2 can be approximated by $I_2 \approx q_{\text{ref}}^2/(2m_\phi^2)$. Thus in the case of a heavy mediator, $G_2(q^2)$ can be reduced to $G_2(q^2) \approx 2q^2/q_{\text{ref}}^2$ which is suppressed by the smallness of q^2 .

Type-III operator \mathcal{O}_6 corresponds to the anapole type of interactions which results in the matrix elements of the form

$$|M_{\chi N}(q^2, v)|^2 \propto \frac{v_\perp^2}{(q^2 + m_\phi^2)^2} \quad (18)$$

For type-III operators, the factor $G_3(q^2, v)$ is given by

$$G_3(q^2, v) = \frac{v_\perp^2/v_{\text{ref}}^2}{I_3(q_{\text{min}}^2/m_\phi^2, q_{\text{ref}}^2/m_\phi^2) (1 + q^2/m_\phi^2)^2} \quad (19)$$

where $I_3(a, b) = I_1(a, b) - I_2(a, b)/b$. In the limit of Eq. (14), the function I_3 can be approximated by $I_3 \approx 1/2 - q_{\text{ref}}^2/(3m_\phi^2)$. Thus in the heavy mediator case, $G_3(q^2, v) \approx 2v_\perp^2/v_{\text{ref}}^2$.

The operators \mathcal{O}_7 , \mathcal{O}_8 and \mathcal{O}_9 contribute dominantly to spin-dependent cross sections. Their subdominant contributions to the spin-independent cross sections can be catalogued into three types (type-IV, -V and -VI). They are suppressed by higher powers of q^2 or v_\perp^2 . Since these operators are now severely constrained by the null-results from PICASSO [71] and COUPP [72], etc., they are not considered in the remainder of this work. The factors $G(q^2, v)$ for these operators are shown in the Appendix. Note that the operators \mathcal{O}_3 , \mathcal{O}_4 , \mathcal{O}_{12} and \mathcal{O}_{14} give no contribution to the spin-independent cross section.

For the operators under consideration, at nucleus level, the spin-independent DM-nucleus differential cross section $d\sigma_A/dq^2$ can be written as follows

$$\frac{d\sigma_A}{dq^2} = \frac{\bar{\sigma}_p}{4\mu_{\chi p}^2 v^2} [Z + \xi(A - Z)]^2 G(q^2, v) F_A^2(q^2), \quad (20)$$

where Z and A are the atomic number and atomic mass number of the target nucleus, respectively, and ξ is the relative strength between DM-neutron and DM-proton coupling. The case where $\xi \neq 1$ corresponding to the isospin violating DM, and for $\xi = -0.7$, the XENON100 constraints can be weakened maximumly, see e.g. [73, 74]. Note that large isospin violating is subject to constraints from the data of cosmic-ray photons [75] and antiprotons [76, 77]. The factor $F_A(q^2)$ is related to the distribution of the nucleon within the nucleus. For type-I, type-II and type-IV operators, it is simply the form factor $F_A(q^2) = F(q^2) = \int d^3x \rho(x) e^{iqx}$ where $\rho(x)$ is the density distribution function of the nucleon inside the nucleus. However, for type-III, type-V and type-VI operators because the nucleon velocity operator \mathbf{v} acting on the nucleus wave function will pick up the nucleus mass, the reduced mass $\mu_{\chi N}$ in the expression of v_\perp in Eq. (10) will be replaced by $\mu_{\chi A}$ (for detailed derivation, see e.g. [69]). This effect can be effectively absorbed into the expression of $F_A(q^2)$ as follows

$$F_A(q^2) = \frac{v^2 - q^2/4\mu_{\chi A}^2}{v^2 - q^2/4\mu_{\chi p}^2} F(q^2). \quad (21)$$

The form factor $F^2(q^2)$ can be taken as the Helm form [78],

$$F^2(q^2) = \frac{9j_1^2(qR_1)}{q^2 R_1^2} e^{-q^2 s^2}, \quad (22)$$

where $j_1(x)$ is the spherical Bessel function, $R_1 = \sqrt{R_A^2 - 5s^2}$ with $R_A \simeq 1.2A^{1/3}$ fm is an effective nuclear radius and $s \simeq 1$ fm.

3 Determination of DM particle mass

For GeV scale WIMP DM particles, the typical momentum transfer q in the DM-nucleus scattering process is at MeV scale. In the case where the value of m_ϕ^2 is comparable with q^2 , the predicted spectrum of dR/dE_R is significantly different from the case with contact interactions and the mass of the DM particle determined from fitting to the measured dR/dE_R becomes sensitive to the value of m_ϕ . The differential recoil event rate per detector mass is given by

$$\frac{dR}{dE_R} = \frac{dN}{M_A dt dE_R} = \frac{2\rho_\chi}{m_\chi} \int_{|\mathbf{v}| > v_{\min}} d^3\mathbf{v} v f(\mathbf{v}) \frac{d\sigma_A}{dq^2}, \quad (23)$$

where $E_R = q^2/(2m_A)$ is the nuclear recoil energy, $\rho_\chi \approx 0.3 \text{ GeV} \cdot \text{cm}^{-3}$ is the local DM energy density, and M_A is the total mass of the target nucleus (in units of kg). The minimal velocity required to generate the recoil energy E_R in elastic scatterings is $v_{\min} = \sqrt{m_A E_R / (2\mu_{\chi A}^2)}$ with $\mu_{\chi A} = m_\chi m_A / (m_\chi + m_A)$ the DM-nucleus reduced mass. The DM velocity distribution function $f(\mathbf{v})$ is related to that in the Galactic frame $f_G(\mathbf{v})$ through a Galilean transformation $f(\mathbf{v}) = f_G(\mathbf{v} + \mathbf{v}_E; v_0, v_{\text{esc}})$, where \mathbf{v}_E is the velocity of the Earth relative to the rest frame of the Galactic halo, $v_0 \approx 220 \text{ km} \cdot \text{s}^{-1}$ is the most probable velocity of the DM particle, and $v_{\text{esc}} \approx 544 \text{ km} \cdot \text{s}^{-1}$ is the Galactic escape velocity from the solar system. The DM velocity distribution in the Galactic halo rest frame is often assumed to be the standard Maxwell-Boltzmann distribution with a cutoff at v_{esc} ,

$$f_G(\mathbf{v}) = \frac{1}{N} \exp\left(-\frac{v^2}{v_0^2}\right) \Theta(v_{\text{esc}} - v), \quad (24)$$

with the normalization constant given by $N = (\pi v_0^2)^{3/2} \text{erf}(v_{\text{esc}}/v_0) - 2v_{\text{esc}} \exp(-v_{\text{esc}}^2/v_0^2) / (\pi v_0^2)$. It is useful to define the slope of the recoil event spectrum as follows

$$S(q^2) \equiv -2m_A \frac{d^2 R / dE_R^2}{dR/dE_R}, \quad (25)$$

which in principle can be determined by experiment, if the statistics of the recoil events is high enough.

For the operators under consideration, the expressions of the recoil event rates involve two type of velocity integrals

$$\begin{aligned} g_1(v_{\min}) &= \int_{v_{\min}} \frac{f(\mathbf{v})}{v} d^3\mathbf{v} \\ &= \frac{1}{2v_E} \left[\text{erf}\left(\frac{v_+}{v_0}\right) - \text{erf}\left(\frac{v_-}{v_0}\right) \right] - \frac{1}{\sqrt{\pi}v_E} \left(\frac{v_+ - v_-}{v_0} \right) e^{-v_{\text{esc}}^2/v_0^2} \end{aligned} \quad (26)$$

and

$$\begin{aligned}
g_2(v_{\min}) &= \int_{v_{\min}} v f(\mathbf{v}) d^3\mathbf{v} \\
&= \frac{v_0}{\sqrt{\pi}} \left[\left(\frac{v_-}{2v_E} + 1 \right) e^{-v_-^2/v_0^2} - \left(\frac{v_+}{2v_E} - 1 \right) e^{-v_+^2/v_0^2} \right] \\
&\quad + \frac{v_0^2}{4v_E} \left(1 + 2\frac{v_E^2}{v_0^2} \right) \left[\operatorname{erf} \left(\frac{v_+}{v_0} \right) - \operatorname{erf} \left(\frac{v_-}{v_0} \right) \right] \\
&\quad - \frac{v_0}{\sqrt{\pi}} \left[2 + \frac{1}{3v_E v_0^2} \left((v_{\min} + v_{\text{esc}} - v_-)^3 - (v_{\min} + v_{\text{esc}} - v_+)^3 \right) \right] e^{-v_{\text{esc}}^2/v_0^2},
\end{aligned} \tag{27}$$

where $v_{\pm} = \min(v_{\min} \pm v_E, v_{\text{esc}})$.

In general, the spectral feature of the differential event rate depends on both m_χ and m_ϕ . Thus the value of m_χ can be determined as a function of m_ϕ . In order to illustrate of the role of m_ϕ in the determination of DM particle mass, we first consider an extreme case where $v_E \ll v_{\min}$ and $v_{\text{esc}} \rightarrow \infty$. In this limit, $f(\mathbf{v}) \approx f_G(\mathbf{v})$ and $g_{1,2}(v_{\min})$ can be approximated by

$$g_1(v_{\min}) \approx \frac{2}{\sqrt{\pi}v_0} e^{-v_{\min}^2/v_0^2} \quad \text{and} \quad g_2(v_{\min}) \approx \frac{2}{\sqrt{\pi}v_0} (v_{\min}^2 + v_0^2) e^{-v_{\min}^2/v_0^2}. \tag{28}$$

Neglecting the q^2 -dependence in the form factor $F(q^2)$, for type-I operators, the differential event rate is given by

$$\left(\frac{dR}{dE_R} \right)_{\text{type-I}} \approx \frac{2C}{\sqrt{\pi}v_0} \frac{1}{(q^2 + m_\phi^2)^2} \exp \left(-\frac{q^2}{4\mu_{\chi A}^2 v_0^2} \right). \tag{29}$$

where $C = \rho_\chi \bar{\sigma}_p [Z + \xi(A - Z)]^2 / (2m_\chi \mu_{\chi p}^2)$ is a constant independent on q^2 . For type-I operators, $S(q^2)$ is nearly a constant, if $m_\phi^2 \gg q^2$. Let us define a quantity $S_{\text{exp}}(q^2)$ which is assumed to be the value of $S(q^2)$ measured by the experiment at a momentum transfer q^2 . For a given $S_{\text{exp}}(q^2)$, the value of m_χ can be determined as a function of m_ϕ as follows

$$m_\chi = \frac{m_A}{v_0 \sqrt{S_{\text{exp}}(q^2) - \frac{8m_A^2}{q^2 + m_\phi^2} - 1}}. \tag{30}$$

The dependences of m_χ on m_ϕ have different behaviour in three parameter regions:

- A) in the region where $8m_A^2/(q^2 + m_\phi^2) \ll S_{\text{exp}}(q^2)$, the determined value of m_χ is almost insensitive to m_ϕ .
- B) in the region where the values of $8m_A^2/(q^2 + m_\phi^2)$ and $S_{\text{exp}}(q^2)$ are of the same order of magnitude, the value of m_χ increases with a decreasing m_ϕ . When m_ϕ^2 is vanishing, the value of m_χ saturates and reaches its maximal value

$$m_{\chi, \text{max}} = \frac{m_A}{v_0 \sqrt{S_{\text{exp}}(q^2) - 8m_A^2/q^2 - 1}}. \tag{31}$$

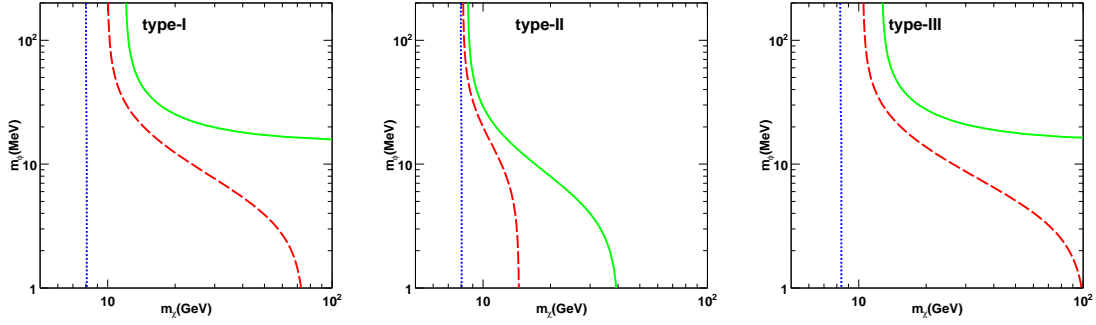


FIG. 1: Relations between m_χ and m_ϕ for three sets of values of S_{exp} and q^2 listed in Eq. (36) for type-I, -II and -III operators. The three curves in each panel corresponds to the case A (blue dotted), B (red dashed) and C (green solid) in Eq. (36), respectively. The target nucleus is assumed to be silicon.

C) in a special parameter region where $S_{\text{exp}}(q^2) - 8m_A^2/(q^2 + m_\phi^2) \approx 1/v_0^2$, the value of m_χ becomes very large and even divergent. Thus in this case, the mass of the DM particle is not constrained by the data.

For Type-II operators, the differential event rate is given by

$$\left(\frac{dR}{dE_R}\right)_{\text{type-II}} \approx \frac{2C}{\sqrt{\pi}v_0} \left(\frac{q^2}{q_{\text{ref}}^2}\right) \frac{1}{(q^2 + m_\phi^2)^2} \exp\left(-\frac{q^2}{4\mu_{\chi A}^2 v_0^2}\right). \quad (32)$$

Similarly, given the value of $S_{\text{exp}}(q^2)$, m_χ as a function of m_ϕ can be obtained as

$$m_\chi = \frac{m_A}{v_0 \sqrt{S_{\text{exp}}(q^2) - \frac{8m_A^2}{q^2 + m_\phi^2} + \frac{4m_A^2}{q^2} - 1}}. \quad (33)$$

Thus for the same values of $S_{\text{exp}}(q^2)$ and m_ϕ , Type-II operators lead to a smaller m_χ compared with Type I operators.

For Type-III operators, the integration over velocity results in a simple relation

$$\int_{v_{\text{min}}}^{\infty} d^3\mathbf{v} \left(\frac{v_\perp^2}{v_{\text{ref}}^2}\right) \frac{f_G(\mathbf{v})}{v} = \frac{2}{\sqrt{\pi}v_0} \left(\frac{v_0^2}{v_{\text{ref}}^2}\right) \exp\left(-\frac{q^2}{4\mu_{\chi A}^2 v_0^2}\right), \quad (34)$$

which shows that in the limit $f(\mathbf{v}) \approx f_G(\mathbf{v})$, the differential event rate has the same q^2 dependence as that in type-I operators. Consequently,

$$\left(\frac{dR}{dE_R}\right)_{\text{type-III}} \approx \left(\frac{v_0^2}{v_{\text{ref}}^2}\right) \left(\frac{dR}{dE_R}\right)_{\text{type-I}} \quad (35)$$

Thus the relation between m_χ and m_ϕ are the same as that for type-I operators in Eq. (30) in the limit of $v_E \ll v_{\text{min}}$ and $v_{\text{esc}} \rightarrow \infty$.

In more realistic cases where v_E is comparable with v_{\min} in size, the full expressions of $g_{1,2}(v_{\min})$ in Eqs.(26)-(27) have to be applied, and the value of the DM particle mass can be determined numerically. For a concrete illustration, we assume that the target nucleus is made of silicon. We consider three reference values of $S_{\text{exp}}(q^2)$, which are chosen according to the three typical cases A, B and C discussed previously.

$$\begin{aligned} A) \quad & S_{\text{exp}} = 5.25 \times 10^7, \text{ at } q^2 = 900 \text{ MeV}^2, \\ B) \quad & S_{\text{exp}} = 1.57 \times 10^7, \text{ at } q^2 = 400 \text{ MeV}^2, \\ C) \quad & S_{\text{exp}} = 1.13 \times 10^7, \text{ at } q^2 = 324 \text{ MeV}^2, \end{aligned} \tag{36}$$

and solve the value of m_χ from Eq. (25) for as a function of m_ϕ . The velocity of the Earth is set to be $v_E \approx v_\odot$ with $v_\odot = v_0 + 12 \text{ km} \cdot \text{s}^{-1}$ being the velocity of the Sun in the Galactic halo rest frame. Thus the effect of solar modulation is neglected. In Fig. 1, the solutions for m_χ for three type of operators are shown. It can be seen that the three reference values of S_{exp} roughly correspond to the three cases of A, B and C discussed in the limit of $v_E \ll v_{\min}$ and $v_{\text{esc}} \rightarrow \infty$. Comparing the results for three different types of operators, one sees that the type-II operators indeed lead to a smaller m_χ than type-I operators for a given m_ϕ . For type-III operators, although the result is quite similar to the case of type-I operators, it predicts a slightly larger m_χ . In DM direct detection experiments, the target nuclei are of different type and the measured spectra can be in a wide range of q^2 (or E_R). However, the observation that a smaller m_ϕ can lead to a larger m_χ is quite general, as it will be shown in the next section.

4 Interpretation of the direct detection data in the light mediator scenario

In the DM direct detection experiments, the measured event signal s could be the electron-recoil equivalent energy E_{ee} , direct scintillation signal S1, and ionization electron charge signal S2, etc.. The differential signal event rate is given by

$$\frac{dR}{ds} = \int_0^\infty dE_R \varepsilon(s) P(s, E_R) \frac{dR}{dE_R}, \tag{37}$$

where $P(s, E_R)$ is the possibility of observing a signal s , given a recoil energy E_R . For a given experiment, the signal s is related to E_R through a function $s = f(E_R)$. For a detector with perfect signal resolution, $P(s, E_R) = \delta(s - f(E_R))$. The efficiency of detecting the signal s is denoted by $\varepsilon(s)$. In the case where $P(s, E_R)$ is Gaussian and ε is

a constant, the expected total event number in a signal range $[s_1, s_2]$ is given by

$$N_{[s_1, s_2]} = \text{Ex} \int_0^\infty dE_R \left(\frac{dR}{dE_R} \right) \frac{\varepsilon}{2} \left[\frac{\text{erf}(s_1 - f(E_R))}{\sqrt{2}\sigma} - \frac{\text{erf}(s_2 - f(E_R))}{\sqrt{2}\sigma} \right], \quad (38)$$

where $\text{Ex} = M_A \Delta t$ is the exposure, and σ is the signal resolution.

In this section, we constrain the parameters related to the DM properties such as m_χ , m_ϕ , ξ and σ_p from the experimental data through evaluating the function $\chi^2 = -\sum 2\ln\mathcal{L}$ with \mathcal{L} being the likelihood function. The likelihood function is chosen according to the extended maximum likelihood method which takes into account the distribution of the signal events for the experiments coming with unbinned data [79]

$$\mathcal{L} = e^{-(N+B)} \prod_i^n \left[\left(\frac{dN}{ds} \right)_i + \left(\frac{dB}{ds} \right)_i \right], \quad (39)$$

where $N(B)$ is the expected total number of signal events from DM (background) in the whole measured recoil energy range. The corresponding differential event rate at the i -th event ($i = 1, \dots, n$) is denoted by $(dN(B)/ds)_i$. We first vary the values of parameters to obtain the minimal value of the χ^2 function χ_{\min}^2 , then calculate $\Delta\chi^2 = \chi^2 - \chi_{\min}^2$ which is assumed to follow a χ^2 distribution. The allowed regions of parameter space at 68%, 90% and 95% CL correspond to $\Delta\chi^2 = 2.3, 4.6$ and 6.0 , respectively, for the case with two degrees of freedom (d.o.f).

4.1 The experimental data

At present, the most stringent constraints on the spin-independent cross sections come from the data of SuperCDMS [11] and LUX [14], which are in strong disagreement with the positive results from DAMA [2, 3] and CoGeNT [4–6]. The CoGeNT result is also challenged by that from the CDEX experiment which utilizes the same type of germanium detector [17], and there are still debates on the uncertainties in the analysis of the CoGeNT data [80, 81]. Only the positive signals from CDMS-II-Si [7] can be marginally consistent with the limits from LUX and SuperCDMS in fine tuned DM models with xenophobic or Ge-phobic interactions. Thus in this work, we shall mainly focus on the interpretation and compatibility of the following three experiments:

- **CDMS-II-Si**, the CDMS-II experiment measures both the ionization electrons and non-equilibrium phonons. Recently, the CDMS-II experiment reported an observation of 3 possible DM-induced events with recoil energies at $E_R=8.2, 9.5$ and 12.3 keV, respectively, in its silicon detectors, based on a raw exposure of 140.2 kg-days [7]. The estimated background from surface event is $0.41_{-0.08}^{+0.20}(\text{stat.})_{-0.24}^{+0.28}(\text{syst.})$ and that from neutrons and ^{206}Pb are < 0.13 and < 0.08 at the 90% CL, respectively. We

take $B = 0.62$ as a conservative estimate and assume a constant dB/dE_R which is normalized to give the total event number B in the recoil energy interval 7–100 keV. The acceptance efficiency is obtained from Fig. 1 of Ref. [7]. For the CDMS-II-Si experiment, a perfect energy resolution is assumed.

- **SuperCDMS**, with an exposure of 577 kg·days, the SuperCDMS experiment observed $N = 11$ nuclear recoil events in the energy range of 1.6–10.0 keV [11]. The estimated total background is $B = 6.1^{+1.1}_{-0.8}$ events. The recoil energies of the 11 events were listed in Tab. 1 of Ref. [11], and the acceptance efficiency $\varepsilon(E_R)$ is obtained from the Fig. 1 of Ref. [11]. Again a perfect energy resolution is assumed for the SuperCDMS experiment.
- **LUX**, the LUX experiment utilizes a dual-phase XENON time-projection chamber which measures both the prompt scintillation signal S1 and ionization electron charge signal S2. With an exposure of 1.01×10^4 kg·days, only one candidate event at S1=3.2 PE (~ 4.9 keV) marginally passed the selection cuts in the S1 signal range 2 – 30 PE [14]. The estimated number of background is $B = 0.64 \pm 0.16$. The event number of S1 signals in a given interval $[S1_a, S1_b]$ is given by

$$N = \int_{S1_a}^{S1_b} dS1 \sum_{s1=1}^{\infty} \varepsilon(S1) \text{Gauss}(S1|s1, \sigma) \int_0^{\infty} \text{Pois}(s1|f(E_R)) \varepsilon_{S2}(E_R) \frac{dR}{dE_R} dE_R, \quad (40)$$

where σ is the energy resolution. For the LUX experiment $\sigma = \sqrt{s1} \sigma_{\text{PMT}}$ with $\sigma_{\text{PMT}} = 0.37$ PE. We read off the S1 detection efficiency $\varepsilon(S1)$ from Fig. 1 of Ref. [14], and $f(E_R)$ from the S1- $\log_{10}(S2/S1)$ plots in Fig. 3 and 4 of Ref. [14]. The candidate event at S1=3.2 PE corresponds to a recoil energy $E_R \simeq 4.9$ keV. An additional S2 efficiency cutoff ε_{S2} for $E_R < 3.0$ keV is adopted [38, 83].

For a comparison purpose, we also calculate upper limits from the following experiments. Unless otherwise stated, the limits are obtained using the maximum gap method [82].

- **CDMSlite**. The exposure of CDMSlite is 6.3 kg·days. The recoil energy spectrum is shown in Fig. 1 of Ref. [10]. We consider the energy range from 0.17 to 7.00 keVee, and use the histogram with bin-width of 10 eVee for the energy spectrum from 0.10 to 1.60 keVee, and the histogram with bin-width of 75 eVee for energy range from 1.60 to 7.00 keVee. The detection efficiency is taken to be 98.5% and the energy resolution is 0.014 keVee. The recoil energy E_R is reconstructed from the electron-recoil equivalent energy E_{ee} the same as defined in Ref. [10]. Since the derivation of upper limits from maximum gap method requires requires unbinned data, Following Ref. [83], we rearrange the data set by dividing each bin with multiple events into smaller equal-size bins so that there is one event in each bin.

- **CDEX** the CDEX-1 experiment utilizes a P-type point-contact germanium detector. The DM search based on a 53.9 kg·days of exposure did not show excess of events over the expected background, and stringent upper limits on DM-nucleus scattering cross section were obtained [17]. For CDEX, we construct a Gaussian likelihood function

$$\mathcal{L} = \prod_i \frac{1}{\sqrt{2\pi}\sigma_{i,\text{exp}}} \exp \left[-\frac{(R_{i,\text{exp}} - R_{i,\text{DM}})^2}{2\sigma_{i,\text{exp}}^2} \right], \quad (41)$$

where for bin i , $R_{i,\text{exp}}$ and $\sigma_{i,\text{exp}}$ are the detected event rate and error per keV·kg-day, which is read off from Fig. 3(b) of Ref. [17], $R_{i,\text{DM}}$ is the theoretical predicted event rate from DM plus a free constant background. The quenching factor is taken from Ref. [84], and a perfect energy resolution is assumed.

- **XENON100**, with an exposure of 225 days \times 34 kg, 2 events were reported as the possible excess, with recoil energies of 7.1 keV (3.3 PE) and 7.8 keV (3.8 PE) [13]. The background expectation is $B = 1.0$ events. The expected spectrum are also calculated using Eq. (40), where we take $f(E_R) = (S_{\text{nr}}/S_{\text{ee}})L_y E_R \mathcal{L}_{\text{eff}}(E_R)$, with $S_{\text{nr}} = 0.95$, $S_{\text{ee}} = 0.58$, and $L_y = 2.28$ [13]. We adopt the measurements of $\varepsilon(\text{S1})$ and \mathcal{L}_{eff} from Ref. [85]. For XENON100 experiment, $\sigma_{\text{PMT}} = 0.5$ PE. An S2 efficiency cutoff ε_{S2} for $E_R < 3.0$ keV is adopted.
- **XENON10**, we use the results of an S2-only analysis on XENON10 [12] with an exposure of 15 kg·days. The recoil energies of the candidate events are read off from Fig. 2 of Ref. [12]. The expected event number in a given energy range $[E_1, E_2]$ is calculated using Eq. (38), where the energy resolution is $\sigma = E_R/\sqrt{E_R Q_y}$. The electron yield Q_y is read off from the solid curve in Fig. 1 of Ref. [12], as that used by the XENON10 collaboration. A cutoff that Q_y vanishes for $E_R < 1.4$ keV is adopted. In the numerical calculation, we adopt a flat efficiency of $\varepsilon = 0.94$.
- **PandaX** is an other dual-phase xenon time-projection chamber located at CJPL. The first DM search results from PandaX-1 were based on a 643.8 kg·days of exposure, and no DM candidate event was found. In this work, the expected spectrum of PandaX is also calculated using Eq. (40). The efficiency cut $\varepsilon(\text{S1})$ is read off from the black curve (the overall NR detection efficiency) in Fig. 3 of Ref. [15]. The values of $f(E_R)$ are read off from the red solid curve in Fig. 5 of Ref. [15]. Furthermore, the upper limits are obtained assuming a Poisson distribution of DM induced events with an expected background of $B = 0.15$ events.

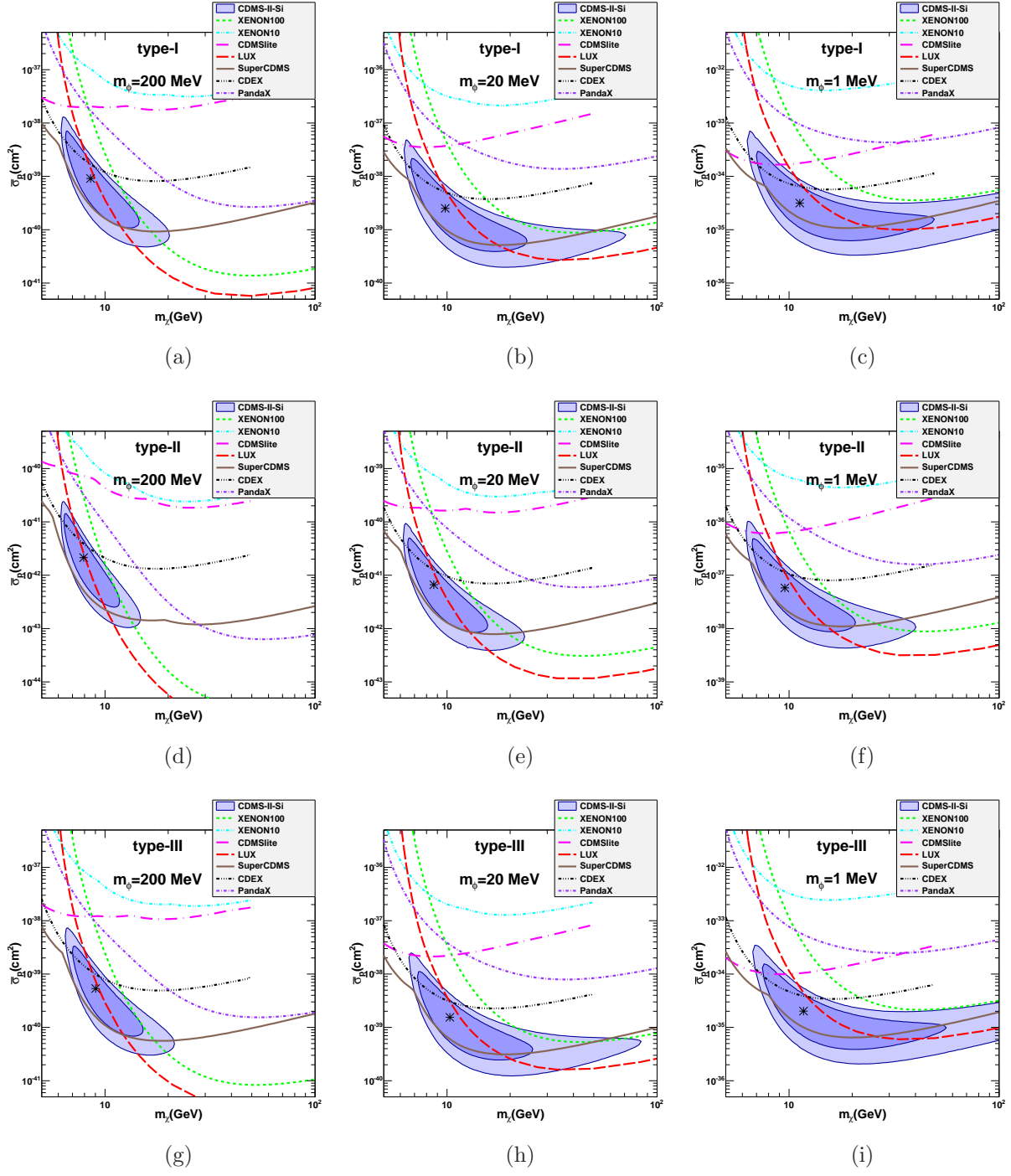


FIG. 2: The 68% and 90% CL favored regions from CDMS-II-Si [7] as well as 90% CL upper limits from XENON100 [13], XENON10 [12], CDMSlite [10], LUX [14], SuperCDMS [11], CDEX [17] and PandaX [15] in the (m_χ, σ_p) plane. The best fit points of CDMS-II-Si are also shown as asterisks. For type-I, II and III operators (from top to bottom) with $m_\phi = 200, 20$ and 1 MeV (from left to right). The isospin violation parameter is fixed at $\xi = -0.7$.

4.2 Results

We first investigate how the presence of a light mediator changes the interpretation of individual DM direct detection experiments, with the focus on the results of CDMS-II-Si. We perform a fit to the CDMS-II-Si data using the likelihood function of Eq. (39) for three typical cases of very light ($m_\phi = 1$ MeV), light ($m_\phi = 20$ MeV), and heavy ($m_\phi = 200$ MeV) mediators. The case with “very light ” mediator corresponds to the mediator mass below the energy threshold of typical DM detection experiments, and the case with “heavy” mediator corresponds to a nearly contact DM-nucleus interaction. The isospin-violation parameter is fixed at $\xi = -0.70$ for future convenience, as in this case the LUX constraint is maximally weakened. Note that in the interpretation of CDMS-II-Si data alone, a different choice of ξ only leads to a rescaling of $\bar{\sigma}_p$. In Fig. 2, the best-fit values of m_χ and $\bar{\sigma}_p$ and the regions favored by the data in the $(m_\chi, \bar{\sigma}_p)$ plane at 68% and 90% CL are shown for the operators of type-I, -II and -III. The effect of light mediators on the 90% CL upper limits of the experiments such as SuperCDMS, CDMSlite, CDEX, LUX, XENON100/10 and PandaX are also calculated and shown in Fig. 2. The upper limits from SuperCDMS is calculated using the maximum gap method. As expected, the value of m_χ favored by the CDMS-II-Si data increases when the mediator becomes lighter, and the upper limits from other experiments becomes weaker towards high DM particle mass.

For type-I operators, the favored value of m_χ changes dramatically with a decreasing m_ϕ . At 68% CL, for a heavy mediator $m_\phi = 200$ MeV, the CDMS-II-Si favored DM particle mass is in the range $\sim 7 - 15$ GeV. For a smaller $m_\phi = 20$ MeV, the allowed value of m_χ can reach ~ 23 GeV. For a tiny $m_\phi = 1$ MeV, it can reach ~ 50 GeV. At 90% CL, the effect of light mediator is even more significant. For $m_\phi = 20$ MeV, the allowed value of m_χ is already larger than 70 GeV. For $m_\phi = 1$ MeV, the value of m_χ can be larger than 100 GeV. As it can be seen from Fig. 2, the upper limits from other experiments also change significantly with different choices of m_ϕ . In general, when the mediator is lighter, the shape of the exclusion curve becomes more flat toward large m_χ region, which indicates that the limits are relatively weaker compared with that at low m_χ region. This effect of light mediator can be clearly seen in the exclusion limits of LUX. For type-I operators, when $m_\phi = 200$ MeV, the LUX limit at $m_\chi = 10$ (50) GeV is $\sim 3 \times 10^{-40}$ (5×10^{-42}) cm^2 , which indicates that the limit at $m_\chi = 50$ GeV is lower than that at 10 GeV by a factor of ~ 60 . When $m_\phi = 20$ MeV, this factor is reduced to ~ 17 , and for $m_\phi = 1$ MeV, this factor is further reduced to ~ 10 . Similar observations can be obtained for other experiments. Although only a small portion of the CDMS-II-Si favoured region is allowed after the constraints from LUX and SuperCDMS, the allowed region is enlarged when m_ϕ is smaller, which shows the possibility that the presence of a

light mediator can relax the tension between these experimental results.

For type-II and type-III operators, the conclusions are similar. For these type of operators, light mediators also enlarge the allowed range for the DM particle mass. For type-II operators, the upper limits on the DM particle mass are $\sim 12(17)$ GeV at 68% (90%) CL for $m_\phi = 200$ MeV, and the upper limits change to $\sim 20(40)$ GeV at 68% (90%) CL for $m_\phi = 1$ MeV. Compared with type-I operators, the allowed DM particle mass is smaller, which is in agreement with the analytical analysis in section 3. For type-III operators, the obtained upper limits are quite similar to the case with type-I operators, which can be understood from Eqs. (34)-(35). The upper limits on the DM particle mass are $\sim 16(22)$ GeV at 68% (90%) CL for $m_\phi = 200$, and the upper limits are $\sim 60(100)$ GeV at 68% (90%) CL for $m_\phi = 1$ MeV.

In the next step, we allow the value of m_ϕ to be free (with a cut off at $m_\phi \geq 0.2$ MeV) and to be determined by fitting the CDMS-II-Si data. The allowed regions of parameter space are shown in (m_χ, m_ϕ) plane and $(m_\chi, \bar{\sigma}_p)$ plane, respectively, in Fig. 3. For all the operators under consideration, the value of m_χ increases with a decreasing m_ϕ . However, at $m_\phi \approx 5$ MeV, the increase saturates, corresponding to the case B in Eq. (36). At 68% CL, the maximally allowed DM particle masses are ~ 40 GeV, ~ 20 GeV and ~ 40 GeV for type-I, type-II and type-III operators, respectively. Note that at higher confidence levels such as 95% CL, the allowed value of m_ϕ can exceed 100 GeV for type-I and type-III operators. Since a small m_ϕ can greatly enhance the scattering amplitude, the allowed range of $\bar{\sigma}_p$ can vary in a large range of a few order of magnitudes. This situation is also shown in Fig. 3.

Finally, we perform a combined χ^2 analysis on the results of the three experiments CDMS-II-Si, SuperCDMS and LUX, and allow all the four parameters m_χ , m_ϕ , $\bar{\sigma}_p$ and ξ to vary. The results of the allowed regions in the parameter space are shown in Fig. 4. It can be seen that after including the results of SuperCDMS and LUX, in general a light mediator with $m_\phi \lesssim 20$ MeV is favored by the data. The allowed mass of DM particle is slightly reduced, but still much larger than the case with contact interaction. The value of isospin-violation parameter ξ is found to be i.e., $\xi = -0.70 \pm 0.02$, very close to xenophobic, which is driven by the LUX data.

For type-I operators, at 68% CL the allowed range of m_χ is $\sim 8 - 23$ GeV. At 90% CL, the allowed m_χ can reach 80 GeV. For type-II operators, at 68% CL, the allowed range of m_χ is $\sim 6 - 13$ GeV. At 90% CL, the allowed m_χ can reach ~ 20 GeV. Note that there is a local minimum at $\xi = -0.78$ and $m_\chi \sim 6$ GeV, which corresponds to the “Ge-phobic” DM [86]. A “Ge-phobic” DM can maximally relax the constraint from SuperCDMS. In the case of type-III operators, the result is similar to the case of type-I operators.

The presence of light mediator can help in relaxing the tensions among the three

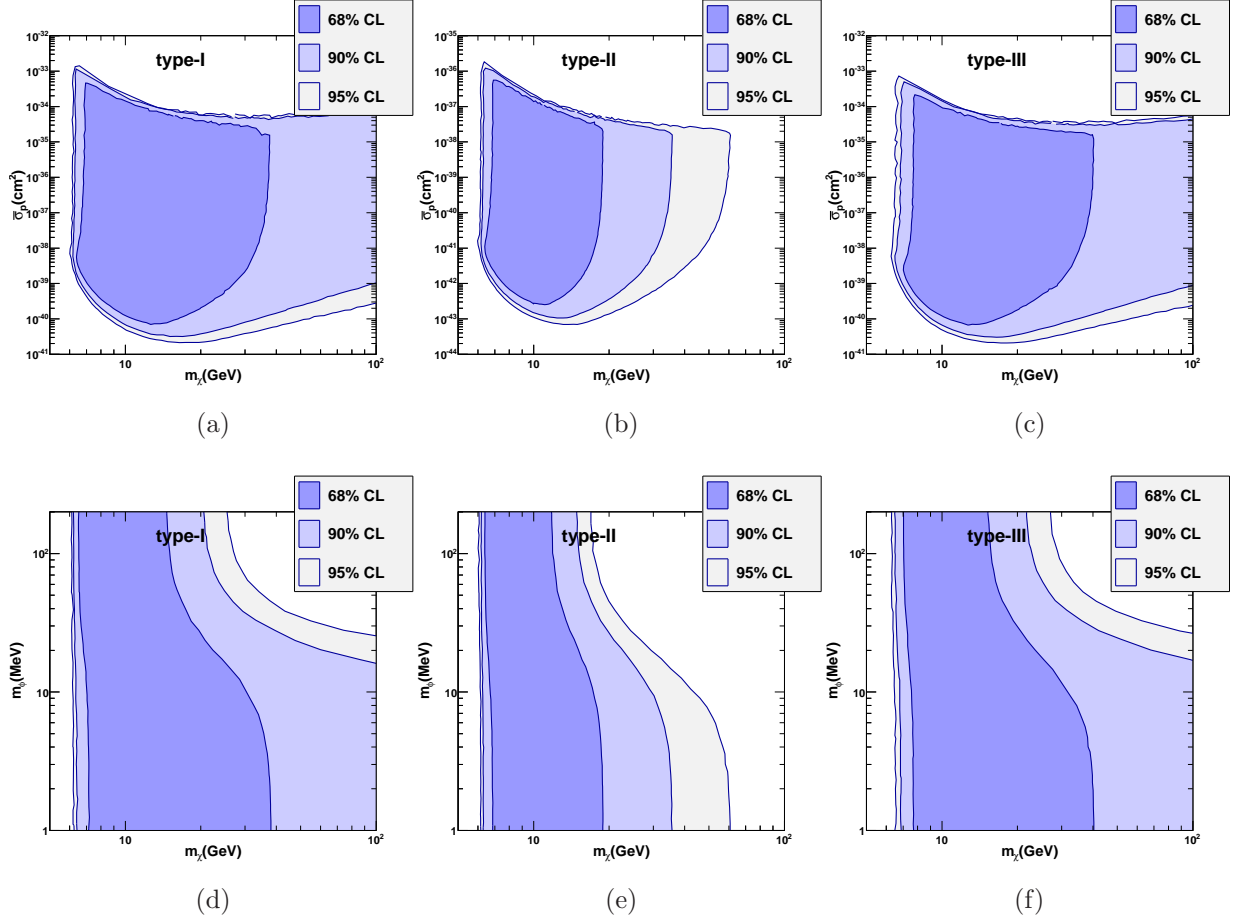


FIG. 3: The regions of parameter space allowed by the CDMS-II-Si data at 68%, 90% and 95% CLs in (m_χ, σ_p) plane (top panels) and (m_χ, m_ϕ) plane (bottom panels) for three type of operators. The isospin-violation parameter is fixed at $\xi = -0.7$.

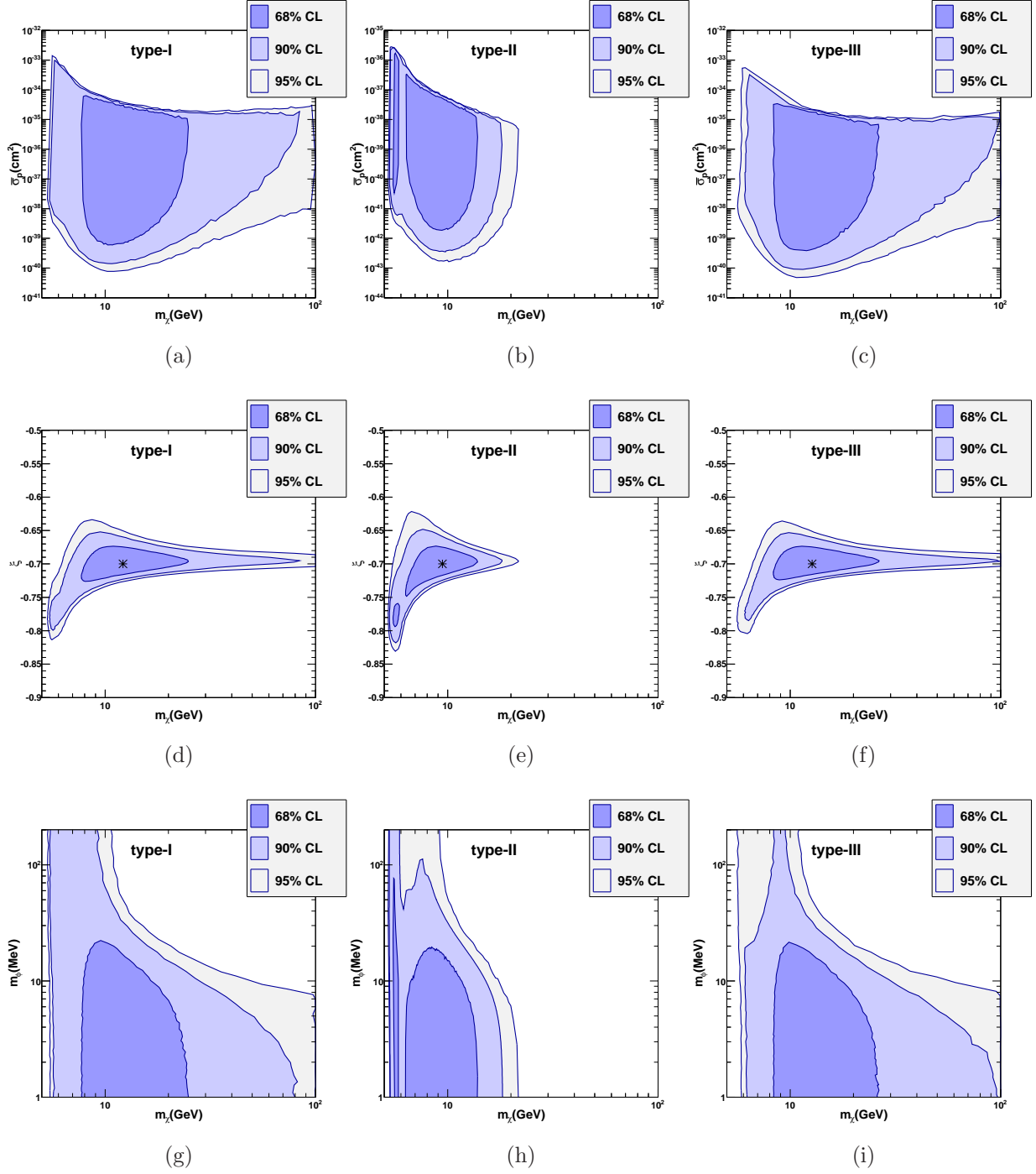


FIG. 4: The favored regions (68%, 90% and 95% CL) from the global fits on the combination of CDMS-II-Si, LUX and SuperCDMS for three type of operators. (Top panels) the favored regions in the (m_χ, σ_p) plane. (Middle panels) the favored regions in the (m_χ, ξ) plane. The best fit points are also shown as asterisks. (Bottom panels) the favored regions in the (m_χ, m_ϕ) plane.

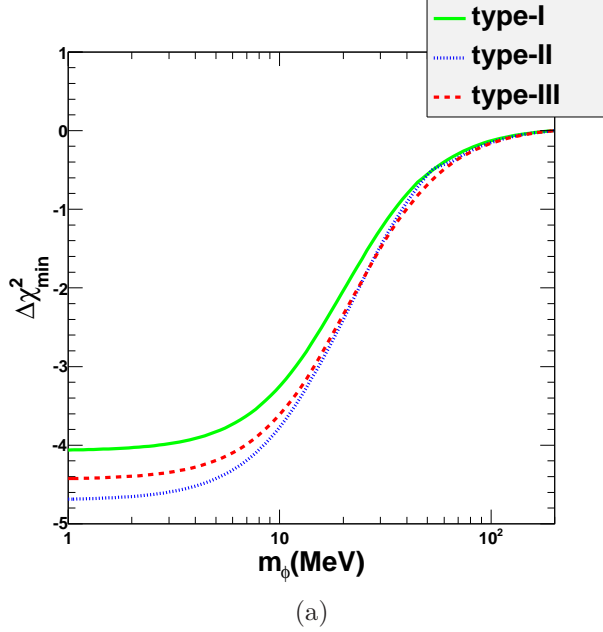


FIG. 5: The value of $\Delta\chi^2_{\min}$ as a function of m_ϕ , based on the global fits on the combination of CDMS-II-Si, LUX and SuperCDMS. The curves correspond to the operators of type-I (green solid), type-II (blue dotted) and type-III (red dashed).

experiments. In Fig. 5, we plot the quantity $\Delta\chi^2_{\min} = \chi^2_{\min}(m_\phi) - \chi^2_{\min}(m_\phi = 200\text{MeV})$ which is the χ^2_{\min} as a function of m_ϕ relative to that at a large $m_\phi = 200$ MeV. The figure shows that for all the three type of operators, the value of $\Delta\chi^2_{\min}$ decreases for a decreasing m_ϕ . One sees that the reduction of $\Delta\chi^2_{\min}$ can be $\sim 4 - 5$.

5 Conclusion

In summary, we have discussed the scenario where the DM particle scatters off target nuclei through the exchange of a light mediator particle. In this case, the spectral feature of the recoil event rate depends on the mass of the mediator and type of interactions, and can be significantly different from the case of contact-like interactions. We have adopted an extended effective operator framework, and discussed the momentum and velocity dependences of the scattering cross sections for all the operators. The interpretation of the current experimental data of CDMS-II-Si, SuperCDMS and LUX, etc. has been discussed with the focus on the determination of DM particle mass for the relevant operators. We have found that in general the allowed DM particle mass from the experimental data increases significantly when the mediator particle becomes lighter. For the data of CDMS-II Si, the allowed DM particle mass can reach $\sim 50(100)$ GeV at 68% (90%) CL depending

on the type of operators, and the increasement saturates when the mediator mass is below $\mathcal{O}(10)$ MeV. The upper limits from other experiments such as SuperCDMS, CDMSlite, CDEX, XENON10/100, LUX, PandaX etc. all become weaker at high DM mass region. In a combined analysis, we have shown that the presence of a light mediator can partially relax the tension in the current results of CDMS-II-Si, SuperCDMS and LUX.

Acknowledgments

This work is supported in part by the National Basic Research Program of China (973 Program) under Grants No. 2010CB833000; the National Nature Science Foundation of China (NSFC) under Grants No. 10821504, No. 11335012 and No. 11475237.

Appendix

A Subdominate spin-independent operators

In this section, we list the $G(q^2, v)$ factors for the subdominant operators $\mathcal{O}_7 - \mathcal{O}_9$. They can be catalogued into the following types.

Type-IV operator \mathcal{O}_9 contributes to the matrix elements of the form

$$|M_{\chi N}(q^2, v)|^2 \propto \frac{q^4}{(q^2 + m_\phi^2)^2}, \quad (42)$$

The $G(q^2, v)$ factor for this type of matrix element is

$$G_4(q^2) = \frac{q^4/m_\phi^4}{I_4(q_{\min}^2/m_\phi^2, q_{\text{ref}}^2/m_\phi^2) (1 + q^2/m_\phi^2)^2}, \quad (43)$$

where

$$I_4(a, b) \equiv \frac{1}{b-a} \int_a^b dt \frac{t^2}{(1+t)^2} = 1 - I_1(a, b) - 2I_2(a, b), \quad (44)$$

In the limit of Eq. (14), the function I_4 has an asymptotic form $I_4 \approx q_{\text{ref}}^2/(3m_\phi^2)$.

Type-V operators \mathcal{O}_8 and \mathcal{O}_9 also contribute to the matrix elements of the form

$$|M_{\chi N}(q^2, v)|^2 \propto \frac{v_\perp^2 q^2}{(q^2 + m_\phi^2)^2}, \quad (45)$$

with

$$G_5(q^2, v) = \frac{v_\perp^2 q^2 / (v_{\text{ref}}^2 m_\phi^2)}{I_5(q_{\min}^2/m_\phi^2, q_{\text{ref}}^2/m_\phi^2) (1 + q^2/m_\phi^2)^2}, \quad (46)$$

where $I_5(a, b) = I_2(a, b) - I_4(a, b)/b$. In the limit of Eq. (14), the function I_5 has an asymptotic form $I_5 \approx q_{\text{ref}}^2/(6m_\phi^2)$.

Type-VI operators \mathcal{O}_7 contribute to the matrix elements of the form

$$|M_{\chi N}(q^2, v)|^2 \propto \frac{v_\perp^2 q^4}{(q^2 + m_\phi^2)^2}, \quad (47)$$

For type-VI operators,

$$G_6(q^2, v) = \frac{v_\perp^2 q^4 / (v_{\text{ref}}^2 m_\phi^4)}{I_6(q_{\text{min}}^2/m_\phi^2, q_{\text{ref}}^2/m_\phi^2) (1 + q^2/m_\phi^2)^2}, \quad (48)$$

where

$$\begin{aligned} I_6(a, b) &\equiv I_4(a, b) - \frac{1}{b(b-a)} \int_a^b dt \frac{t^3}{(1+t)^2} \\ &= \frac{ab(a+b) + (b-a)^2 - 3(a+b) - 6}{2b(1+a)(1+b)} + \frac{3}{b(b-a)} \ln \left(\frac{1+b}{1+a} \right). \end{aligned} \quad (49)$$

References

- [1] **Planck Collaboration** Collaboration, P. Ade et al., *Planck 2013 results. XVI. Cosmological parameters*, *Astron.Astrophys.* **571** (2014) A16, [[arXiv:1303.5076](#)].
- [2] **DAMA Collaboration** Collaboration, R. Bernabei et al., *First results from DAMA/LIBRA and the combined results with DAMA/NaI*, *Eur.Phys.J.* **C56** (2008) 333–355, [[arXiv:0804.2741](#)].
- [3] **DAMA Collaboration, LIBRA Collaboration** Collaboration, R. Bernabei et al., *New results from DAMA/LIBRA*, *Eur.Phys.J.* **C67** (2010) 39–49, [[arXiv:1002.1028](#)].
- [4] C. Aalseth, P. Barbeau, J. Colaresi, J. Collar, J. Diaz Leon, et al., *Search for an Annual Modulation in a P-type Point Contact Germanium Dark Matter Detector*, *Phys.Rev.Lett.* **107** (2011) 141301, [[arXiv:1106.0650](#)].
- [5] **CoGeNT Collaboration** Collaboration, C. Aalseth et al., *CoGeNT: A Search for Low-Mass Dark Matter using p-type Point Contact Germanium Detectors*, *Phys.Rev.* **D88** (2013), no. 1 012002, [[arXiv:1208.5737](#)].
- [6] **CoGeNT Collaboration** Collaboration, C. Aalseth et al., *Search for An Annual Modulation in Three Years of CoGeNT Dark Matter Detector Data*, [[arXiv:1401.3295](#)].

- [7] **CDMS Collaboration** Collaboration, R. Agnese et al., *Silicon Detector Dark Matter Results from the Final Exposure of CDMS II*, *Phys.Rev.Lett.* **111** (2013) 251301, [[arXiv:1304.4279](#)].
- [8] **CDMS Collaboration** Collaboration, D. Akerib et al., *A low-threshold analysis of CDMS shallow-site data*, *Phys.Rev.* **D82** (2010) 122004, [[arXiv:1010.4290](#)].
- [9] **CDMS-II Collaboration** Collaboration, Z. Ahmed et al., *Results from a Low-Energy Analysis of the CDMS II Germanium Data*, *Phys.Rev.Lett.* **106** (2011) 131302, [[arXiv:1011.2482](#)].
- [10] **SuperCDMS Collaboration** Collaboration, R. Agnese et al., *Search for Low-Mass Weakly Interacting Massive Particles Using Voltage-Assisted Calorimetric Ionization Detection in the SuperCDMS Experiment*, *Phys.Rev.Lett.* **112** (2014), no. 4 041302, [[arXiv:1309.3259](#)].
- [11] **SuperCDMS Collaboration** Collaboration, R. Agnese et al., *Search for Low-Mass Weakly Interacting Massive Particles with SuperCDMS*, *Phys.Rev.Lett.* **112** (2014), no. 24 241302, [[arXiv:1402.7137](#)].
- [12] **XENON10 Collaboration** Collaboration, J. Angle et al., *A search for light dark matter in XENON10 data*, *Phys.Rev.Lett.* **107** (2011) 051301, [[arXiv:1104.3088](#)].
- [13] **XENON100 Collaboration** Collaboration, E. Aprile et al., *Dark Matter Results from 225 Live Days of XENON100 Data*, *Phys.Rev.Lett.* **109** (2012) 181301, [[arXiv:1207.5988](#)].
- [14] **LUX Collaboration** Collaboration, D. Akerib et al., *First results from the LUX dark matter experiment at the Sanford Underground Research Facility*, *Phys.Rev.Lett.* **112** (2014), no. 9 091303, [[arXiv:1310.8214](#)].
- [15] **PandaX Collaboration** Collaboration, M. Xiao et al., *First dark matter search results from the PandaX-I experiment*, *Sci.China Phys.Mech.Astron.* **57** (2014) 2024–2030, [[arXiv:1408.5114](#)].
- [16] **SIMPLE Collaboration** Collaboration, M. Felizardo et al., *The SIMPLE Phase II Dark Matter Search*, *Phys.Rev.* **D89** (2014) 072013, [[arXiv:1404.4309](#)].
- [17] **CDEX Collaboration** Collaboration, Q. Yue et al., *Limits on light WIMPs from the CDEX-1 experiment with a p-type point-contact germanium detector at the China Jinping Underground Laboratory*, *Phys.Rev.* **D90** (2014), no. 9 091701, [[arXiv:1404.4946](#)].

- [18] H. Goldberg and L. J. Hall, *A New Candidate for Dark Matter*, *Phys.Lett.* **B174** (1986) 151.
- [19] K. Cheung and T.-C. Yuan, *Hidden fermion as milli-charged dark matter in Stueckelberg Z- prime model*, *JHEP* **0703** (2007) 120, [[hep-ph/0701107](#)].
- [20] D. Feldman, Z. Liu, and P. Nath, *The Stueckelberg Z-prime Extension with Kinetic Mixing and Milli-Charged Dark Matter From the Hidden Sector*, *Phys.Rev.* **D75** (2007) 115001, [[hep-ph/0702123](#)].
- [21] M. Pospelov and T. ter Veldhuis, *Direct and indirect limits on the electromagnetic form-factors of WIMPs*, *Phys.Lett.* **B480** (2000) 181–186, [[hep-ph/0003010](#)].
- [22] K. Sigurdson, M. Doran, A. Kurylov, R. R. Caldwell, and M. Kamionkowski, *Dark-matter electric and magnetic dipole moments*, *Phys.Rev.* **D70** (2004) 083501, [[astro-ph/0406355](#)].
- [23] S. Gardner, *Shedding Light on Dark Matter: A Faraday Rotation Experiment to Limit a Dark Magnetic Moment*, *Phys.Rev.* **D79** (2009) 055007, [[arXiv:0811.0967](#)].
- [24] J. H. Heo, *Minimal Dirac Fermionic Dark Matter with Nonzero Magnetic Dipole Moment*, *Phys.Lett.* **B693** (2010) 255–258, [[arXiv:0901.3815](#)].
- [25] E. Masso, S. Mohanty, and S. Rao, *Dipolar Dark Matter*, *Phys.Rev.* **D80** (2009) 036009, [[arXiv:0906.1979](#)].
- [26] V. Barger, W.-Y. Keung, and D. Marfatia, *Electromagnetic properties of dark matter: Dipole moments and charge form factor*, *Phys.Lett.* **B696** (2011) 74–78, [[arXiv:1007.4345](#)].
- [27] S. Chang, N. Weiner, and I. Yavin, *Magnetic Inelastic Dark Matter*, *Phys.Rev.* **D82** (2010) 125011, [[arXiv:1007.4200](#)].
- [28] W. S. Cho, J.-H. Huh, I.-W. Kim, J. E. Kim, and B. Kyae, *Constraining WIMP magnetic moment from CDMS II experiment*, *Phys.Lett.* **B687** (2010) 6–10, [[arXiv:1001.0579](#)].
- [29] T. Banks, J.-F. Fortin, and S. Thomas, *Direct Detection of Dark Matter Electromagnetic Dipole Moments*, [arXiv:1007.5515](#).
- [30] J.-F. Fortin and T. M. Tait, *Collider Constraints on Dipole-Interacting Dark Matter*, *Phys.Rev.* **D85** (2012) 063506, [[arXiv:1103.3289](#)].

- [31] K. Kumar, A. Menon, and T. M. Tait, *Magnetic Fluffy Dark Matter*, *JHEP* **1202** (2012) 131, [[arXiv:1111.2336](#)].
- [32] V. Barger, W.-Y. Keung, D. Marfatia, and P.-Y. Tseng, *Dipole Moment Dark Matter at the LHC*, *Phys.Lett.* **B717** (2012) 219–223, [[arXiv:1206.0640](#)].
- [33] E. Del Nobile, C. Kouvaris, P. Panci, F. Sannino, and J. Virkajarvi, *Light Magnetic Dark Matter in Direct Detection Searches*, *JCAP* **1208** (2012) 010, [[arXiv:1203.6652](#)].
- [34] N. Weiner and I. Yavin, *How Dark Are Majorana WIMPs? Signals from MiDM and Rayleigh Dark Matter*, *Phys.Rev.* **D86** (2012) 075021, [[arXiv:1206.2910](#)].
- [35] C. M. Ho and R. J. Scherrer, *Anapole Dark Matter*, *Phys.Lett.* **B722** (2013) 341–346, [[arXiv:1211.0503](#)].
- [36] A. L. Fitzpatrick and K. M. Zurek, *Dark Moments and the DAMA-CoGeNT Puzzle*, *Phys.Rev.* **D82** (2010) 075004, [[arXiv:1007.5325](#)].
- [37] M. T. Frandsen, F. Kahlhoefer, C. McCabe, S. Sarkar, and K. Schmidt-Hoberg, *The unbearable lightness of being: CDMS versus XENON*, *JCAP* **1307** (2013) 023, [[arXiv:1304.6066](#)].
- [38] M. I. Gresham and K. M. Zurek, *Light Dark Matter Anomalies After LUX*, *Phys.Rev.* **D89** (2014) 016017, [[arXiv:1311.2082](#)].
- [39] J. Hewett, H. Weerts, R. Brock, J. Butler, B. Casey, et al., *Fundamental Physics at the Intensity Frontier*, [arXiv:1205.2671](#).
- [40] J. Jaeckel, *A force beyond the Standard Model - Status of the quest for hidden photons*, *Frascati Phys.Ser.* **56** (2012) 172–192, [[arXiv:1303.1821](#)].
- [41] R. Essig, J. A. Jaros, W. Wester, P. H. Adrian, S. Andreas, et al., *Working Group Report: New Light Weakly Coupled Particles*, [arXiv:1311.0029](#).
- [42] T. Schwetz and J. Zupan, *Dark Matter attempts for CoGeNT and DAMA*, *JCAP* **1108** (2011) 008, [[arXiv:1106.6241](#)].
- [43] N. Fornengo, P. Panci, and M. Regis, *Long-Range Forces in Direct Dark Matter Searches*, *Phys.Rev.* **D84** (2011) 115002, [[arXiv:1108.4661](#)].
- [44] R. C. Cotta, A. Rajaraman, T. M. P. Tait, and A. M. Wijangco, *Particle Physics Implications and Constraints on Dark Matter Interpretations of the CDMS Signal*, *Phys.Rev.* **D90** (2014) 013020, [[arXiv:1305.6609](#)].

- [45] D. Curtin, Z. Surujon, and Y. Tsai, *Direct Detection with Dark Mediators*, *Phys.Lett.* **B738** (2014) 477–482, [[arXiv:1312.2618](#)].
- [46] H. An, L.-T. Wang, and H. Zhang, *Dark matter with t -channel mediator: a simple step beyond contact interaction*, *Phys.Rev.* **D89** (2014) 115014, [[arXiv:1308.0592](#)].
- [47] **PAMELA Collaboration** Collaboration, O. Adriani et al., *An anomalous positron abundance in cosmic rays with energies 1.5-100 GeV*, *Nature* **458** (2009) 607–609, [[arXiv:0810.4995](#)].
- [48] O. Adriani, G. Barbarino, G. Bazilevskaya, R. Bellotti, M. Boezio, et al., *A statistical procedure for the identification of positrons in the PAMELA experiment*, *Astropart.Phys.* **34** (2010) 1–11, [[arXiv:1001.3522](#)].
- [49] **Fermi LAT Collaboration** Collaboration, M. Ackermann et al., *Measurement of separate cosmic-ray electron and positron spectra with the Fermi Large Area Telescope*, *Phys.Rev.Lett.* **108** (2012) 011103, [[arXiv:1109.0521](#)].
- [50] **AMS Collaboration** Collaboration, L. Accardo et al., *High Statistics Measurement of the Positron Fraction in Primary Cosmic Rays of 0.5500 GeV with the Alpha Magnetic Spectrometer on the International Space Station*, *Phys.Rev.Lett.* **113** (2014), no. 12 121101.
- [51] H.-B. Jin, Y.-L. Wu, and Y.-F. Zhou, *Implications of the first AMS-02 measurement for dark matter annihilation and decay*, *JCAP* **1311** (2013) 026, [[arXiv:1304.1997](#)].
- [52] H.-B. Jin, Y.-L. Wu, and Y.-F. Zhou, *Cosmic ray propagation and dark matter in light of the latest AMS-02 data*, [arXiv:1410.0171](#).
- [53] A. Sommerfeld, *Annalen der Physik*, 403, 257 (1931).
- [54] J. Hisano, S. Matsumoto, and M. M. Nojiri, *Unitarity and higher order corrections in neutralino dark matter annihilation into two photons*, *Phys.Rev.* **D67** (2003) 075014, [[hep-ph/0212022](#)].
- [55] J. Hisano, S. Matsumoto, and M. M. Nojiri, *Explosive dark matter annihilation*, *Phys.Rev.Lett.* **92** (2004) 031303, [[hep-ph/0307216](#)].
- [56] M. Cirelli, A. Strumia, and M. Tamburini, *Cosmology and Astrophysics of Minimal Dark Matter*, *Nucl.Phys.* **B787** (2007) 152–175, [[arXiv:0706.4071](#)].
- [57] N. Arkani-Hamed, D. P. Finkbeiner, T. R. Slatyer, and N. Weiner, *A Theory of Dark Matter*, *Phys.Rev.* **D79** (2009) 015014, [[arXiv:0810.0713](#)].

- [58] M. Pospelov and A. Ritz, *Astrophysical Signatures of Secluded Dark Matter*, *Phys.Lett.* **B671** (2009) 391–397, [[arXiv:0810.1502](#)].
- [59] J. D. March-Russell and S. M. West, *WIMPonium and Boost Factors for Indirect Dark Matter Detection*, *Phys.Lett.* **B676** (2009) 133–139, [[arXiv:0812.0559](#)].
- [60] R. Iengo, *Sommerfeld enhancement: General results from field theory diagrams*, *JHEP* **0905** (2009) 024, [[arXiv:0902.0688](#)].
- [61] S. Cassel, *Sommerfeld factor for arbitrary partial wave processes*, *J.Phys.* **G37** (2010) 105009, [[arXiv:0903.5307](#)].
- [62] J. Chen and Y.-F. Zhou, *The 130 GeV gamma-ray line and Sommerfeld enhancements*, *JCAP* **1304** (2013) 017, [[arXiv:1301.5778](#)].
- [63] Z.-P. Liu, Y.-L. Wu, and Y.-F. Zhou, *Sommerfeld enhancements with vector, scalar and pseudoscalar force-carriers*, *Phys.Rev.* **D88** (2013) 096008, [[arXiv:1305.5438](#)].
- [64] A. Loeb and N. Weiner, *Cores in Dwarf Galaxies from Dark Matter with a Yukawa Potential*, *Phys.Rev.Lett.* **106** (2011) 171302, [[arXiv:1011.6374](#)].
- [65] S. Tulin, H.-B. Yu, and K. M. Zurek, *Beyond Collisionless Dark Matter: Particle Physics Dynamics for Dark Matter Halo Structure*, *Phys.Rev.* **D87** (2013), no. 11 115007, [[arXiv:1302.3898](#)].
- [66] M. Kaplinghat, S. Tulin, and H.-B. Yu, *Direct Detection Portals for Self-interacting Dark Matter*, *Phys.Rev.* **D89** (2014) 035009, [[arXiv:1310.7945](#)].
- [67] S. Chang, A. Pierce, and N. Weiner, *Momentum Dependent Dark Matter Scattering*, *JCAP* **1001** (2010) 006, [[arXiv:0908.3192](#)].
- [68] J. Fan, M. Reece, and L.-T. Wang, *Non-relativistic effective theory of dark matter direct detection*, *JCAP* **1011** (2010) 042, [[arXiv:1008.1591](#)].
- [69] A. L. Fitzpatrick, W. Haxton, E. Katz, N. Lubbers, and Y. Xu, *The Effective Field Theory of Dark Matter Direct Detection*, *JCAP* **1302** (2013) 004, [[arXiv:1203.3542](#)].
- [70] J. Kumar and D. Marfatia, *Matrix element analyses of dark matter scattering and annihilation*, *Phys.Rev.* **D88** (2013), no. 1 014035, [[arXiv:1305.1611](#)].
- [71] **PICASSO Collaboration** Collaboration, S. Archambault et al., *Constraints on Low-Mass WIMP Interactions on ^{19}F from PICASSO*, *Phys.Lett.* **B711** (2012) 153–161, [[arXiv:1202.1240](#)].

- [72] **COUPP Collaboration** Collaboration, E. Behnke et al., *First Dark Matter Search Results from a 4-kg CF₃I Bubble Chamber Operated in a Deep Underground Site*, *Phys.Rev.* **D86** (2012), no. 7 052001, [[arXiv:1204.3094](#)].
- [73] J. L. Feng, J. Kumar, D. Marfatia, and D. Sanford, *Isospin-Violating Dark Matter*, *Phys.Lett.* **B703** (2011) 124–127, [[arXiv:1102.4331](#)].
- [74] M. T. Frandsen, F. Kahlhoefer, J. March-Russell, C. McCabe, M. McCullough, et al., *On the DAMA and CoGeNT Modulations*, *Phys.Rev.* **D84** (2011) 041301, [[arXiv:1105.3734](#)].
- [75] J. Kumar, D. Sanford, and L. E. Strigari, *New Constraints on Isospin-Violating Dark Matter*, *Phys.Rev.* **D85** (2012) 081301, [[arXiv:1112.4849](#)].
- [76] H.-B. Jin, S. Miao, and Y.-F. Zhou, *Implications of the latest XENON100 and cosmic ray antiproton data for isospin violating dark matter*, *Phys.Rev.* **D87** (2013) 016012, [[arXiv:1207.4408](#)].
- [77] Y.-F. Zhou, *Direct and indirect constraints on isospin-violating dark matter*, *Nucl.Phys.Proc.Suppl.* **246-247** (2014) 99–105, [[arXiv:1212.2043](#)].
- [78] J. Lewin and P. Smith, *Review of mathematics, numerical factors, and corrections for dark matter experiments based on elastic nuclear recoil*, *Astropart.Phys.* **6** (1996) 87–112.
- [79] R. J. Barlow, *Extended maximum likelihood*, *Nucl.Instrum.Meth.* **A297** (1990) 496–506.
- [80] C. Aalseth, P. Barbeau, J. Colaresi, J. D. Leon, J. Fast, et al., *Maximum Likelihood Signal Extraction Method Applied to 3.4 years of CoGeNT Data*, [arXiv:1401.6234](#).
- [81] J. H. Davis, C. McCabe, and C. Boehm, *Quantifying the evidence for Dark Matter in CoGeNT data*, *JCAP* **1408** (2014) 014, [[arXiv:1405.0495](#)].
- [82] S. Yellin, *Finding an upper limit in the presence of unknown background*, *Phys.Rev.* **D66** (2002) 032005, [[physics/0203002](#)].
- [83] E. Del Nobile, G. B. Gelmini, P. Gondolo, and J.-H. Huh, *Update on Light WIMP Limits: LUX, lite and Light*, *JCAP* **1403** (2014) 014, [[arXiv:1311.4247](#)].
- [84] **TEXONO Collaboration** Collaboration, S. Lin et al., *New limits on spin-independent and spin-dependent couplings of low-mass WIMP dark matter with a germanium detector at a threshold of 220 eV*, *Phys.Rev.* **D79** (2009) 061101, [[arXiv:0712.1645](#)].

- [85] **XENON100 Collaboration** Collaboration, E. Aprile et al., *Response of the XENON100 Dark Matter Detector to Nuclear Recoils*, *Phys.Rev.* **D88** (2013) 012006, [[arXiv:1304.1427](#)].
- [86] G. B. Gelmini, A. Georgescu, and J.-H. Huh, *Direct detection of light Ge-phobic” exothermic dark matter*, *JCAP* **1407** (2014) 028, [[arXiv:1404.7484](#)].